Synthesis of Palladium Nanoparticles and Their Applications for Surface-Enhanced Raman Scattering and Electrocatalysis

ARTICLE *in* THE JOURNAL OF PHYSICAL CHEMISTRY C · NOVEMBER 2010

Impact Factor: 4.77 · DOI: 10.1021/jp106623y

Synthesis of Palladium Nanoparticles and Their Applications for Surface-Enhanced Raman Scattering and Electrocatalysis

Hongjun Chen,[†] Gang Wei,[‡] Adriana Ispas,[†] Stephen G. Hickey,[†] and Alexander Eychmüller*[,†]

Physikalische Chemie/Elektrochemie, TU Dresden, Bergstr. 66 b, 01062 Dresden, Germany, and Institute of Materials Science & Technology, Friedrich-Schiller-University Jena, Löbdergraben 32, D-07743 Jena, Germany

Received: July 16, 2010; Revised Manuscript Received: November 9, 2010

The synthesis of Pd nanoparticles (NPs) in solution and on surfaces through a seed-mediated growth route is reported. For the Pd NPs synthesized in solution, the diameters of the Pd NPs can be readily tuned from 33 to 110 nm, maintaining good monodispersities by using different amounts of ca. 3 nm gold NPs as seeds. The Pd NPs synthesized are polyhedral in shape and are mainly bounded by {111} facets. They also show a much higher intensity ratio of the (111) to (200) diffraction peaks in comparison to that of the JCPDS card 05-0681. When used as surface-enhanced Raman scattering (SERS) substrates, these Pd NPs show different SERS enhancement as a function of their size, Pd NPs of about 62 nm showing the highest SERS enhancement among the three different sizes of Pd NPs employed in this study. The procedure proposed here to grow Pd NPs in solution can also be used to grow small Pd NPs on gold-sputtered substrates, which display facile electrocatalytic ability for O_2 reduction.

Introduction

Metal nanoparticles (NPs), especially those of the noble metals, are of wide interest not only because of their large surface areas but also because of their specific functions and potential applications, which are different from those of the bulk metal solids.[1] The intrinsic properties of the noble metal NPs are mainly determined by their size, shape, composition, and crystallinity.[2] As a result, the application of size- and shape-control methodologies to the synthesis of noble metal NPs has received considerable attention in recent years. Until now, various synthetic strategies such as hydrothermal methods,[3] photochemical methods,[4] seed-mediated growth methods,[5] polyol reduction methods,[2a,6] and thermal decomposition methods[7] have been demonstrated to be viable routes to the production of noble metal NPs with well-controlled sizes and shapes. Among these well-developed methods, the seed-mediated growth method is one of most convenient and popular strategies and therefore has gained increasing attention. Because the seed-mediated growth method can take place at room temperature, in the presence of air and water, and, in principle, is amenable to upscaling, many noble metal NPs in the form of spheres,[8] cubes,[9] rods,[5] plates,[10] and even core/shell nanostructures[11] have been successfully synthesized using this method.

Palladium plays a key role in many technologies and is employed in many industrial applications, especially those concerned with the low-temperature reduction of automobile pollutants and the formation of C−C bonds in a number of important organic reactions such as Heck, Suzuki, and Stille coupling reactions.[12] Pd is also an important material component in applications involving hydrogen storage and gas sensing.[13] In addition, Pd NPs show high catalytic activity for ethanol electrooxidation in basic media[14] and have the potential to be used as a surface-enhanced Raman scattering (SERS) substrate, where the SERS enhancement intensity has been shown to be size- and morphology-dependent.[15] Thus, the development of new synthetic methods for the formation of Pd NPs with well-controlled size and shape is important for a large number of future applications.

In this work, we present a facile and effective seed-mediated growth route for the controllable synthesis of Pd NPs, polyhedral in shape and mainly bound by {111} facets. Furthermore, the dimensions of the resultant Pd NPs can be readily tailored from 33 to 110 nm, while maintaining good monodispersities through the addition of different amounts of gold seeds. When used as SERS substrates, the Pd NPs with sizes of about 62 nm display the highest SERS enhancement when compared to two other different sizes of Pd NPs prepared in this study (i.e., 110 and 33 nm). The route presented here can also be applied to grow Pd NPs on gold-sputtered substrates and the modified substrate, which contains small Pd NPs; thus obtained, they show good electrocatalytic ability for O_2 reduction.

Experimental Section

Chemicals. Palladous chloride, sodium citrate, and 4-mercaptobenzoic acid (MBA) were purchased from Sigma-Aldrich. Hydrogen peroxide solution (30.62% w/v) was purchased from Fisher Scientific UK Ltd. All reagents were used as received without further purification. The water used was purified through a Millipore system.

Preparation of the Gold-Sputtered Substrates. The gold-sputtered substrate was prepared by thermal evaporation using an evaporation device from Malz & Schmidt (Germany). The evaporation was carried out at a reduced pressure of 10^{-4} Pa. The Au source was of 99.99% purity (Chempur). First, a 5 nm thin layer of Cr was thermally evaporated onto the glass substrates, to provide better adhesion for the Au layer, and then ca. 150 nm Au was evaporated on the top.

Seed-Mediated Synthesis of Pd NPs in Solution and on a Surface. Preparation of ~3 nm gold "seed colloid" solution was performed according to the literature.[16] The formation of

* Corresponding author. E-mail: alexander.eychmueller@chemie.tu-dresden.de.
[†] TU Dresden.
[‡] Friedrich-Schiller-University Jena.

10.1021/jp106623y
Published on Web 11/29/2010

the gold colloidal particles was followed using the UV−vis spectroscopy, and the Au NPs so formed possess a strong surface plasmon band at 512 nm characteristic of colloidal gold.

In a typical Pd NP synthesis, 5 mL of 2 mM H_2PdCl_4 solution and 0.5 mL of 1% sodium citrate solution were added into three different vials (labeled 1, 2, and 3) under magnetic stirring and 200 μL of H_2O_2 (30.62% w/v) added. After complete mixing was achieved, different volumes of the gold seed solution (20, 100, and 500 μL) were added to the vials until the color of the solutions changed from yellow to gray. Finally, the suspensions obtained were centrifuged at different rotation speeds for 10 min, and the solid was washed with Milli-Q water. This centrifugation was followed by rinsing and was repeated three times. For the synthesis of Pd NPs on the gold surface, a similar procedure was used, only replacing the colloidal Au with a gold-sputtered substrate (area approximately 1 × 1.3 cm), and mild shaking was used instead of magnetic stirring.

Instrumentation. The X-ray diffraction (XRD) patterns were collected on a Siemens D5000 X-ray diffractometer using Cu K1 line (1.54 Å, 40 kV, 200 mA) radiation. The XRD samples were prepared by placing several drops of the colloidal solution onto a clean glass plate. Energy-dispersive X-ray analysis (EDX) and scanning electron microscopy (SEM) were performed on a Zeiss DSM 982 Gemini instrument. The samples for SEM and EDX characterization were prepared by transferring the as-prepared products onto silicon substrates. Transmission electron microscopy (TEM) images were obtained using a JEOL 3010 electron microscope operating at 300 kV. SERS spectra were recorded on a Renishaw RM 2000 using the 633 line of a HeNe laser. A CCD camera was employed as detector, using 30 s accumulation time and an incident power of 1 mW. The SERS active substrates were fabricated by transferring the as-prepared Pd NPs of different sizes onto silicon substrates, followed by the addition of 5 μL of a 10^{-4} M MBA solution and waiting until the solvent had evaporated.

Cyclic voltammetry was performed at room temperature with a PAR 273 potentiostat (EG&G, USA) in conventional three-electrode mode with a gold-sputtered substrate or a gold-sputtered substrate onto which Pd NPs had been grown as the working electrode, a large platinum foil as the auxiliary electrode, and a Ag/AgCl (3 M KCl) electrode as the reference electrode against which all potential values within are reported.

Results and Discussion

Synthesis and Characterization of the Pd NPs in Solution and Their Application as SERS Substrates. H_2O_2 has been used as the reducing agent for the fabrication of biosensors based on the biocatalytic growth of gold NPs.[17] It has the advantage that, as compared to other reducing agents, H_2O_2 may be considered to be a clean reducing agent since excess H_2O_2 gradually decomposes into H_2O and O_2, which do not contaminate the resulting products. Figure 1a−c shows typical SEM and TEM images of the NPs, while Figure 1d−f give the particle size distribution histograms corresponding to samples 1, 2, and 3, respectively. As is evident from this figure, the images show the presence of NPs which are monodisperse, weakly agglomerated, and uniform and polyhedral in shape. The mean size of the NPs decreases from 110 nm (sample 1) to 33 nm (sample 3) as the amount of gold seeds increases. A little aggregation is present in Figure 1c. This aggregation may be due to the hydrophobic surface of the TEM grid because no aggregation is observed in the other two samples (Figure 1a,b) where silicon substrates were used for SEM characterization. From the control experiments it is observed that no Pd NPs are formed without the addition of gold seeds under otherwise identical experimental conditions, sufficiently demonstrating that H_2O_2 is a weak reducing agent and cannot produce Pd nucleation under such conditions. The mean particle sizes and the particle-size distributions for samples 1, 2, and 3, as determined from the SEM and TEM images, are summarized in Table 1. The relative standard deviation of these three samples, which is within 8.2−12.1% of the mean particle sizes, confirms the narrow size distribution of these three samples.

To investigate the crystal structure of the Pd NPs, XRD measurements were performed. As shown in Figure 2a, all the diffraction peaks observed can be assigned to the (111), (200), (220), (311), and (222) diffraction peaks of the face-centered cubic (fcc) structure of metallic Pd, respectively. The lattice constant calculated from this XRD pattern is 3.894 Å, which is consistent with that of the reported data (α = 3.889 Å, JCPDS File: 05-0681). Moreover, it is found that the intensity ratio between the (111) and (200) diffraction peaks, $I_{(111)}/I_{(200)}$, is strongly enhanced compared to that of the JCPDS card 05-0681 (29.4 and 7.68 versus 2.38 for samples 1 and 3, respectively), which indicates that the Pd NPs are highly crystalline and mainly bounded by {111} facets. The chemical composition of the Pd NPs was also investigated by EDX as shown in Figure 2b with all peaks being assigned to elemental Pd or Si and C, which stem from the substrate and any adsorbed citrate ions, respectively. In the XRD and EDX data, no trace of Au is detected, indicating that all the Au colloids added act as seeds in the formation of Pd NPs. On the basis of the previous studies of the seed-mediated growth mechanism,[5,8−11] it has been postulated that the presence of Au seeds can catalyze the reduction of $PdCl_4^{2-}$ ions by H_2O_2 because of particle-mediated electron transfer from H_2O_2 to $PdCl_4^{2-}$.[8b] It is well-known that surface energies associated with different crystallographic planes are usually different, and a general sequence of $\gamma\{111\} < \gamma\{100\} < \gamma\{110\}$ may hold. Therefore, it is commonly accepted that the shape of an fcc nanocrystal is mainly determined by the ratio of the growth rate along the [100] versus that of the [111] direction.[18] In this system, because of the fact that the {111} facet of the fcc of Pd has the lowest surface energy and citrate ions probably preferentially adsorb on the sites of the {111} facet, the growth of Pd NPs obviously slows the growth on the {111} facet and promotes a highly anisotropic crystal growth along the other two directions.[3c] Thus, {111}-faceted Pd NPs are eventually formed. Recently, it has also been found that seeding with faceted nanocrystals can have a significant influence on the development of shape-controlled heterostructrues with defined interfaces, for instance, using cubic Pt nanocrystals as seeds for the conformal shape-controlled epitaxial overgrowth of Pd and using 30 nm Au nanooctahedra as the cores to overgrow uniform Au@Pd and Au@Ag nanocubes.[11] Therefore, we infer that the formation of different polyhedral Pd NPs may still have some relationship with the crystal structure of the Au seeds used.

It has been well reported that SERS activity depends not only on the nature of the metal but also on the size, shape, and spacing of the metal NPs. Pd, as one of the transition metals, shows much weaker SERS activity than that of traditional SERS-active metals such as Ag, Au, and Cu.[15a] To investigate the size effect of the Pd NPs on the SERS activity, uniform Pd NPs of three different sizes were synthesized and employed as SERS substrates using 4-mercaptobenzoic acid (MBA) as the Raman probe. Figure 3 presents and compares the SERS signal intensities of the MBA obtained from the Pd NPs of three different sizes at an excitation wavelength of 633 nm. As can

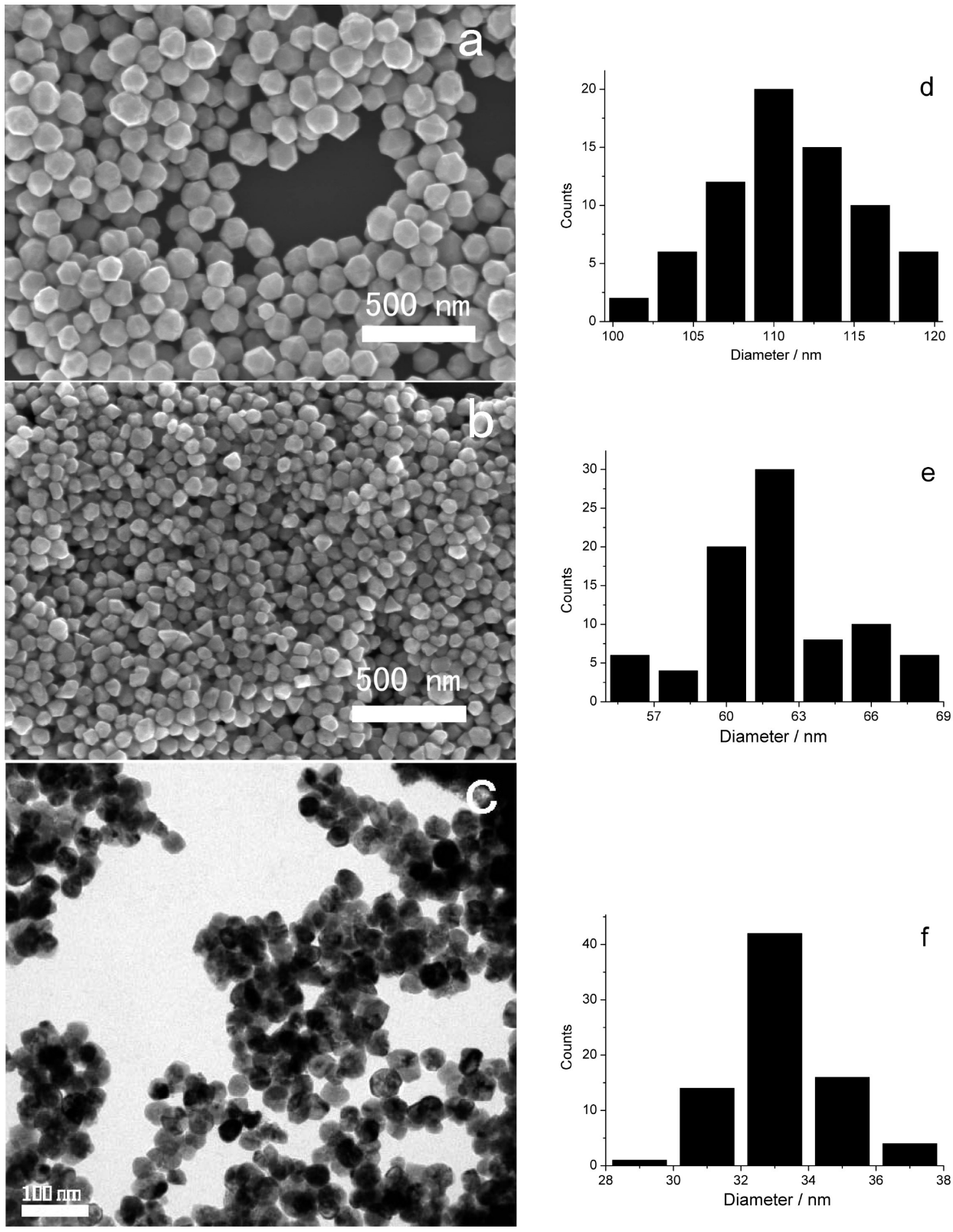

Figure 1. Typical SEM (a and b) and TEM (c) images and their corresponding particle size distribution histograms (d, e, and f) of Pd NPs corresponding to samples 1, 2, and 3, respectively.

be observed, all the spectra measured are consistent with the fingerprint features of the SERS spectrum of MBA in which the typical peaks located at 1587 and 1072 cm^{-1} are assigned to the ν_{8a} and ν_{12} aromatic ring vibrations of MBA.[19] It can also be clearly seen that the SERS enhancement is different for the three samples and the trend from highest intensity to lowest

TABLE 1: Data for the Seed-Mediated Synthesis of Pd NPs

sample	mean particle size/nm	relative standard deviation (%)
1	110 ± 9	8.2
2	62 ± 6	9.7
3	33 ± 4	12.1

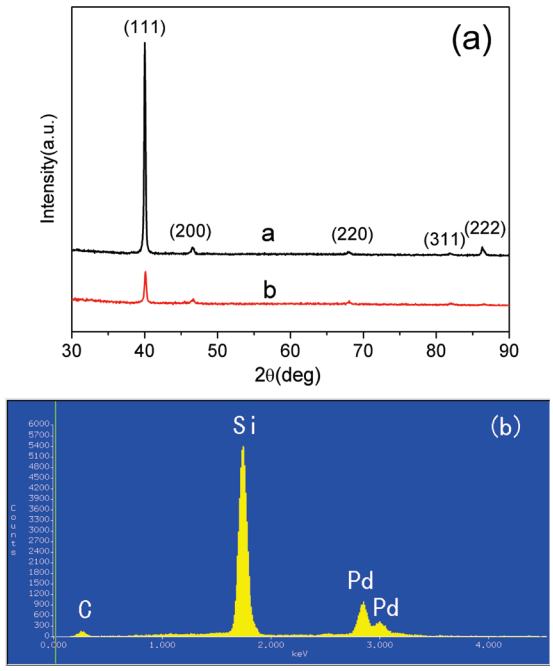

Figure 2. XRD (a) and EDX (b) of the Pd NPs, curves a and b in image (a) corresponding to samples 1 and 3, respectively.

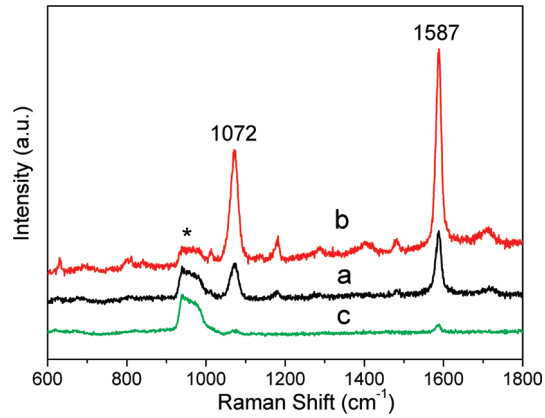

Figure 3. SERS spectra of MBA on Pd NPs: sample 1 (a), sample 2 (b), and sample 3 (c). The peak labeled "*" comes from the underlying Si substrate.

is in the following order: 62 nm Pd NPs > 110 nm Pd NPs > 33 nm Pd NPs. Because of the large thickness of the Pd shell (≥15 nm), it should be pointed out that the SERS activity mainly arises from the Pd overlayer itself rather than the Au core underneath, which is based on the following two considerations: (1) the Au core is too small and has very weak SERS activity because of the surface plasmons being more "off" resonance with the 633 nm laser excitation used here, and (2) when the Pd shell is thicker than 10 nm, these Pd NPs exhibit almost the same SERS activity as the roughened Pd electrode.[15a] On the basis of the reports published by the group of Nie,[20] it is known that the SERS enhancement is directly related to the size of the NPs and the excitation wavelength. The optimal size for Ag NPs to achieve the maximum SERS enhancement under 488 nm excitation is about 70 nm[20a,c] while that for Au NPs under 633 nm excitation is about 60 nm.[20b] In this study, we compared the SERS enhancement of the three different sizes of Pd NPs at 633 nm excitation and found that Pd NPs with ~62 nm in diameter show the highest SERS enhancement.

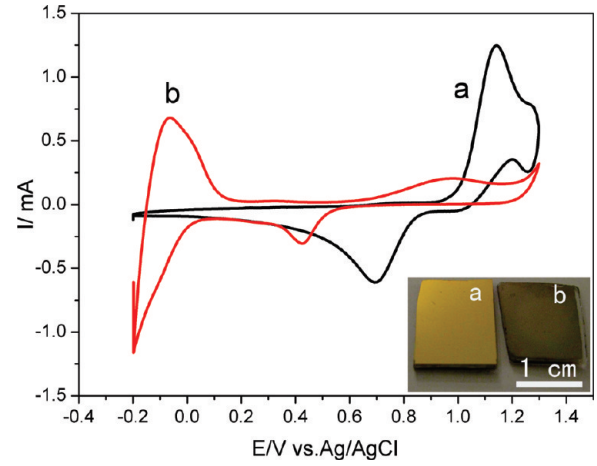

Figure 4. Cyclic voltammograms of the gold-sputtered substrate (a) and Pd NP modified gold-sputtered substrate (b) in N_2-saturated 0.5 M H_2SO_4 at a scan rate of 50 mV s^{-1}. The inset is a photographic comparison of the gold-sputtered substrate (a) and Pd NP modified gold-sputtered substrate (b).

Synthesis and Characterization of Pd NPs on Surfaces and Their Electrocatalytic Ability for O_2 Reduction. In contrast to Pd NPs in solution, the union of Pd NPs as functional materials with solid supports is an important requirement if their deployment in device architectures is to be facilitated. Surfaces modified with Pd NPs are of significance because of their potential in sensing, catalytic, and electrocatalytic applications.[12−14] We therefore sought and achieved a means by which the seed-mediated growth route to the synthesis of the Pd NPs in solution employed above may also be effectively used to grow Pd NPs onto a gold-sputtered substrate. In comparison to conventional methods of using molecular linkers to assemble Pd NPs on solid surfaces, the Pd NP modified solid substrates in the present study are more stable and the deposition easier to control. In addition, because of the fact that Pd NPs are directly grown onto the gold-sputtered substrate, therefore omitting the linkers, the IR drop of such a substrate is expected to be greatly reduced when used as a working electrode in electrochemical applications. As shown in the inset of Figure 4, the color of the gold-sputtered substrate changes from golden to gray, demonstrating that Pd NPs have been successfully grown onto the substrate. To study the effective coverage of the Pd NPs on the substrate, cyclic voltammetry (CV) as a surface-sensitive technique was used. Figure 4 shows cyclic voltammograms of a gold-sputtered substrate (curve a) and Pd NP modified gold-sputtered substrate (curve b) in 0.5 M H_2SO_4, respectively. For the gold-sputtered substrate, the oxide formation initiated at ca. 1.0 V and the oxide removal at ca. 0.7 V, which are typical features of gold electrochemistry,[4c,15a] can be seen. However, the above features are not observed in the case of the Pd NP modified gold-sputtered substrate. This observation clearly demonstrates that the Pd shells essentially cover the entire gold cores and that the substrates are without any notable amount of exposure of gold substrate sites and hence the Pd NP modified gold-sputtered substrate is a pinhole-free surface. For the Pd NP modified gold-sputtered substrate, a broad anodic peak centered at ca. 0.95 V and a cathodic peak at ca. 0.43 V appear (curve b) in the cyclic voltammogram trace, which can be attributed to the oxidation and subsequent reduction of the Pd NPs. In addition, the pair of anodic and cathodic peaks that appear in the potential region −0.2 to 0.1 V are due to hydrogen adsorption and desorption. Such a current−potential profile contains all the typical features associated with Pd electrochemistry.[15a,21]

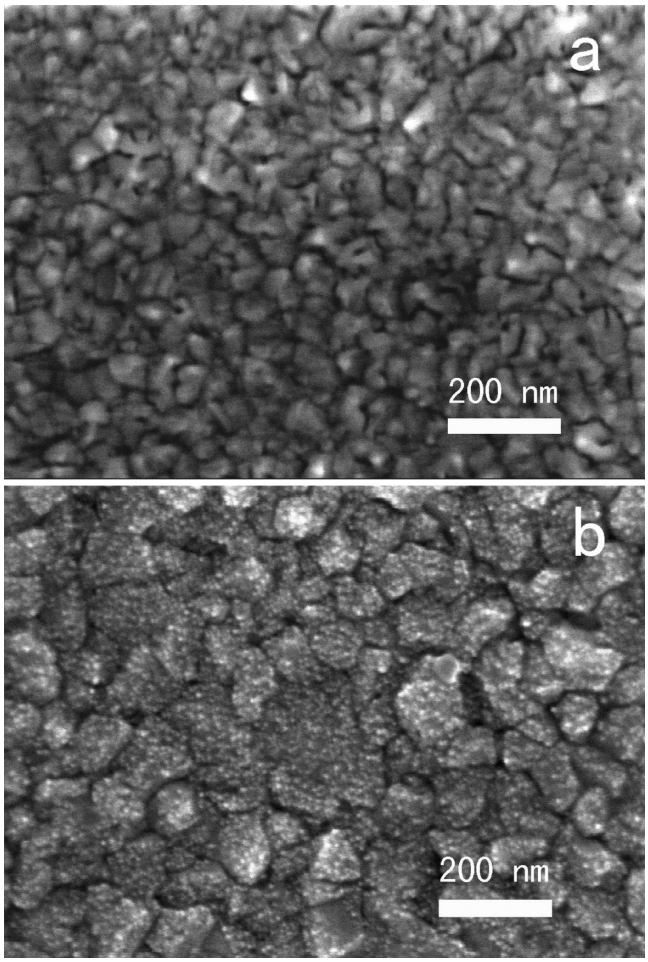

Figure 5. Typical SEM images of a gold-sputtered substrate (a) and Pd NP modified gold-sputtered substrate (b).

To examine the morphology change, SEM was used to characterize the gold-sputtered substrate before and after Pd NP deposition. As shown in Figure 5a, the Au NPs cannot be clearly seen on the gold-sputtered substrate because of the small sizes of Au NPs and the resolution limits of the SEM instrument. In contrast, many Pd NPs are visible as white spots, which can be clearly observed on the gold-sputtered substrate after Pd NP deposition (Figure 5b). The Pd NPs grown on the gold-sputtered substrate have a uniform size of about 6−7 nm in diameter.

To study the electrocatalytic activity of the Pd NPs, further electrochemical measurements were performed. Cyclic voltammograms of a gold-sputtered substrate (curve b) and Pd NPs grown on the gold-sputtered substrate (curve d) in air-saturated 0.5 M H_2SO_4 at a scan rate of 50 mV s^{-1} are shown in Figure 6. Curves a and c correspond to cyclic voltammograms of the gold-sputtered substrate and Pd NPs modified gold-sputtered substrate in N_2-saturated 0.5 M H_2SO_4, respectively. In the presence of O_2, the gold-sputtered substrate shows only a small reduction peak initiated at ca. 0 V (curve b), while the reduction peak initiated at ca. 0.65 V (curve d) for Pd NPs grown on the gold-sputtered substrate, which is more positive than that for a Pd NP-modified glassy carbon electrode and a Ag−Pd bimetallic nanostructure modified indium tin oxide electrode.[4c,22] This clearly demonstrates that Pd NPs grown on the gold-sputtered substrates exhibit good electrocatalytic activity toward O_2 reduction.

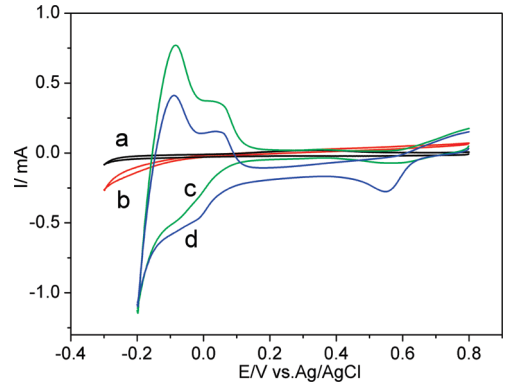

Figure 6. Cyclic voltammograms of the gold-sputtered substrate (curves a and b) and Pd NP modified gold-sputtered substrate (curves c and d) in N_2-saturated (curves a and c) and air-saturated (curves b and d) 0.5 M H_2SO_4 at a scan rate of 50 mV s^{-1}.

Conclusion

We reported on a seed-mediated growth route to the synthesis of Pd NPs in solution and on surfaces. The sizes of the Pd NPs can be readily tuned from 33 to 110 nm and have a uniform distribution. Different sizes of Pd NPs exhibit different degrees of SERS enhancement, with Pd NPs of ~62 nm in diameter displaying the highest SERS enhancement. It is also demonstrated that this route can also be effectively utilized to grow Pd NPs onto gold-sputtered substrates, which subsequently show good electrocatalytic ability for O_2 reduction. It is expected that this route can be developed for other noble metals and further find more widespread applications in the areas of catalysis, fuel cell, and other technologically relevant fields.

Acknowledgment. H.C. appreciates the support from the Alexander von Humboldt (AvH) Foundation. The authors are grateful to Ellen Kern for the SEM images and to Christoph Ziegler for the acquisition of the SERS data.

References and Notes

(1) Feldheim, D. L.; Foss, C. *Metal Nanoparticles: Synthesis, Characterization, and Applications*; Dekker: New York, 2002.

(2) (a) Sun, Y.; Xia, Y. *Science* **2002**, *298*, 2176. (b) Millstone, J. E.; Park, S.; Shuford, K. L.; Qin, L.; Schatz, G. C.; Mirkin, C. A. *J. Am. Chem. Soc.* **2005**, *127*, 5312.

(3) (a) Yu, D.; Yam, W-W. V. *J. Am. Chem. Soc.* **2004**, *126*, 13200. (b) Huang, X.; Zheng, N. *J. Am. Chem. Soc.* **2009**, *131*, 4602. (c) Chen, H.; Wang, Y.; Dong, S. *Inorg. Chem.* **2007**, *46*, 10587.

(4) (a) Jin, R.; Cao, Y. C.; Mirkin, C. A.; Kelly, K. L.; Schatz, G. C.; Zheng, J. G. *Science* **2001**, *294*, 1901. (b) Kim, F.; Song, J. H.; Yang, P. *J. Am. Chem. Soc.* **2002**, *124*, 14316. (c) Chen, H.; Jia, J.; Dong, S. *Nanotechnology* **2007**, *18*, 245601.

(5) (a) Murphy, C. J.; Sau, T. K.; Gole, A. M.; Orendorff, C. J.; Gao, J.; Gou, L.; Hunyadi, S. E.; Li, T. *J. Phys. Chem. B* **2005**, *109*, 13857. (b) Murphy, C. J.; Jana, N. R. *Adv. Mater.* **2002**, *14*, 80. (c) Chen, Y.-H.; Hung, H.-H.; Huang, M. H. *J. Am. Chem. Soc.* **2009**, *131*, 9114.

(6) (a) Xiong, Y.; Chen, J.; Wiley, B.; Xia, Y. *J. Am. Chem. Soc.* **2005**, *127*, 7332. (b) Kim, F.; Connor, S.; Song, H.; Kuykendall, T.; Yang, P. *Angew. Chem., Int. Ed.* **2004**, *43*, 3673. (c) Li, C.; Sato, R.; Kanehara, M.; Zeng, H.; Bando, Y.; Teranishi, T. *Angew. Chem., Int. Ed.* **2009**, *48*, 6883.

(7) (a) Wang, C.; Daimon, H.; Lee, Y.; Kim, J.; Sun, S. *J. Am. Chem. Soc.* **2007**, *129*, 6974. (b) Kim, S.-W.; Park, J.; Jang, Y.; Chung, Y.; Hwang, S.; Hyeon, T. *Nano Lett.* **2003**, *3*, 1289. (c) Teng, X.; Liang, X.; Maksimuk, S.; Yang, H. *Small* **2006**, *2*, 249.

(8) (a) Jana, N. R.; Gearheart, L.; Murphy, C. J. *Langmuir* **2001**, *17*, 6782. (b) Lu, L.; Wang, H.; Xi, S.; Zhang, Ho. *J. Mater. Chem.* **2002**, *12*, 156.

(9) Niu, W.; Li, Z.; Shi, L.; Liu, X.; Li, H.; Han, S.; Chen, J.; Xu, G. *Cryst. Growth Des.* **2008**, *8*, 4440.

(10) (a) Ledwith, D. M.; Whelan, A. M.; Kelly, J. M. *J. Mater. Chem.* **2007**, *17*, 2459. (b) Lu, L.; Kobayashi, A.; Tawa, K.; Ozaki, Y. *Chem. Mater.* **2006**, *18*, 4894.

(11) (a) Habas, S. E.; Lee, H.; Radmilovic, V.; Somorjai, G. A.; Yang, P. *Nat. Mater.* **2007**, *6*, 692. (b) Fan, F.; Liu, D.; Wu, Y.; Duan, S.; Xie, Z.; Jiang, Z.; Tian, Z. *J. Am. Chem. Soc.* **2008**, *130*, 6949.

(12) (a) Moreno-Mañas, M.; Pleixats, R. *Acc. Chem. Res.* **2003**, *36*, 638. (b) Astruc, D. *Inorg. Chem.* **2007**, *46*, 1884. (c) Nishihata, Y.; Mizuki, J.; Akao, T.; Tanaka, H.; Uenishi, M.; Kimura, M.; Okamoto, T.; Hamada, N. *Nature* **2002**, *418*, 164. (d) Alonso, F.; Beletskaya, I. P.; Yus, M. *Chem. Rev.* **2002**, *102*, 4009.

(13) (a) Tobiska, P.; Hugaon, O.; Trouillet, A.; Gagnaire, H. *Sens. Actuators B* **2001**, *74*, 168. (b) Kishore, S.; Nelson, J. A.; Adair, J. H.; Eklund, P. C. *J. Alloys Compd.* **2005**, *389*, 234. (c) Favier, F.; Walter, E. C.; Zach, M. P.; Benter, T.; Penner, R. M. *Science* **2001**, *293*, 2227.

(14) Bianchini, C.; Shen, P. K. *Chem. Rev.* **2009**, *109*, 4183.

(15) (a) Hu, J.; Li, J.; Ren, B.; Wu, D.; Sun, S.; Tian, Z. *J. Phys. Chem. C* **2007**, *111*, 1105. (b) McLellan, J. M.; Xiong, Y.; Hu, M.; Xia, Y. *Chem. Phys. Lett.* **2006**, *417*, 230. (c) Li, Y.; Lu, G.; Wu, X.; Shi, G. *J. Phys. Chem. B* **2006**, *110*, 24585.

(16) (a) Grabar, K. C.; Allison, K. J.; Baker, B. E.; Bright, R. M.; Brown, K. R.; Freeman, R. G.; Fox, A. P.; Keating, C. D.; Musick, M. D.; Natan, M. J. *Langmuir* **1996**, *12*, 2353. (b) Jin, Y. D.; Kang, X. F.; Song, Y. H.; Zhang, B. L.; Cheng, G. J.; Dong, S. *J. Anal. Chem.* **2001**, *73*, 2843.

(17) (a) Zayats, M.; Baron, R.; Popov, I.; Willner, I. *Nano Lett.* **2005**, *5*, 21. (b) Shang, L.; Chen, H.; Deng, L.; Dong, S. *Biosens. Bioelectron.* **2008**, *23*, 1180.

(18) Wang, Z. L. *J. Phys. Chem. B* **2000**, *104*, 1153.

(19) (a) Xu, S.; Ji, X.; Xu, W.; Li, X.; Wang, L.; Bai, Y.; Zhao, B.; Ozaki, Y. *Analyst* **2004**, *129*, 63. (b) Orendorff, C. J.; Tapan, A. G.; Sau, K.; Murphy, C. *J. Anal. Chem.* **2005**, *77*, 3261.

(20) (a) Emory, S. R.; Haskins, W. E.; Nie, S. *J. Am. Chem. Soc.* **1998**, *120*, 8009. (b) Krug, J. T.; Wang, G. D.; Emory, S. R.; Nie, S. *J. Am. Chem. Soc.* **1999**, *121*, 9208. (c) Maxwell, D. J.; Emory, S. R.; Nie, S. *Chem. Mater.* **2001**, *13*, 1082.

(21) Kessler, T.; Visintin, A.; Bolzan, A. E.; Andreasen, G.; Salvarezza, R. C.; Triaca, W. E.; Arvia, A. J. *Langmuir* **1996**, *12*, 6587.

(22) Liu, J.; Cheng, L.; Song, Y.; Liu, B.; Dong, S. *Langmuir* **2001**, *17*, 6747.

JP106623Y